Surface Science 182 (1987) 41–55
North-Holland, Amsterdam

AES, XPS AND EELS STUDY OF THE INITIAL OXIDATION OF POLYCRYSTALLINE CHROMIUM

C. PALACIO *, H.J. MATHIEU and D. LANDOLT

Materials Department, Swiss Federal Institute of Technology, 34 Chemin de Bellerive, CH-1007 Lausanne, Switzerland

Received 15 July 1986; accepted for publication 23 October 1986

The interaction of oxygen with a clean polycrystalline chromium surface has been studied at 300 K in the 10^{-8}–10^{-6} Torr pressure range by means of AES, XPS and EELS. From the chemical information obtained by these analytical techniques, the reaction of the oxygen with the chromium surface has been found to occur in three stages: Dissociative chemisorption of oxygen up to 1–2 L exposures. Nucleation of Cr_2O_3 islands which grow laterally until coalescence up to ~10 L exposures. Beyond 10 L the thickening of the oxide becomes slow and follows a logarithmic law. The beginning of the second stage is characterized by abrupt changes in the chromium AES, XPS and EELS spectra. Also, changes in the energetic position of the AES oxygen peak and of the O1s band have been found during this stage. After the coalescence is reached the average thickness of the film is ~3.8 monolayers. The beginning of the third stage is characterized by an abrupt decrease in the reaction rate leading to a logarithmic type growth law.

1. Introduction

The corrosion and oxidation resistance of iron and nickel alloys is intimately related to their chromium content. A detailed study of the oxidation kinetics of chromium is therefore of theoretical as well as of practical interest. Surface analytical techniques such as Auger electron spectroscopy (AES), X-ray induced photoelectron spectroscopy (XPS) and others are particularly well suited for the investigation of the low temperature oxidation processes and a number of studies employing these techniques with monocrystalline and polycrystalline chromium substrates have appeared in the literature [1–10]. However, published results show a considerable amount of disagreement [2]. In addition no quantitative approach to the study of the first stages of the oxidation process of chromium has been described.

The aim of the present study is to use AES, EELS and XPS to obtain chemical information on the first stages of the interaction of oxygen with a

* Permanent address: Departamento de Física Aplicada, Facultad de Ciencias, C-XII, Universidad Autonoma de Madrid, Cantoblanco, 28049 Madrid, Spain.

0039-6028/87/$03.50

clean polycrystalline chromium surface and to carry out a quantitative analysis of the first stages of the oxidation process.

2. Experimental

A chromium substrate of 99.996% nominal purity (Materials Research) of cylindrical shape (diameter ~ 1 cm, height ~ 1 mm) was used throughout this work. It was mechanically polished with 0.25 μm diamond paste (Buehler) and degreased by successively boiling in carbon tetrachloride, acetone and ethanol. Then the sample was mounted on a heatable transfer bloc and introduced into the UHV chamber via a fast entry-lock. The residual base pressure of the analysis chamber was $\sim 10^{-10}$ Torr. The sample was sputter cleaned "in situ" with 2 keV Kr^+ until no impurities were detected by AES.

Analysis was performed in a AES/XPS system (Perkin-Elmer, model PHI 550/590 A) interfaced to a micro-computer (DEC-PDP 11/34). In AES, a constant primary electron beam current of 0.2 μA at 3 keV primary beam energy was used. To decrease the current density the electron beam was rastered over an area of 70×70 μm^2. The energy resolution was $\Delta E/E \simeq 0.6\%$ and a modulation voltage 1 V_{pp} was supplied to the CMA except for the O KLL and Cr LMM peak, where 3 V_{pp} was used. In EELS, the primary beam energy of 500 eV was applied at a primary electron beam current of 80 nA. In XPS, a monoanode X-ray source was operated a 10 keV, 40 mA current emission using Mg Kα (1253.4 eV) radiation. The binding energy was calibrated using Au $4f_{7/2}$ at 84.0 eV and Cu $2p_{3/2}$ at 932.6 eV. The pass energy of the analyser was 50 eV giving a constant energy resolution $\Delta E = 1$ eV. The sample was positioned at an angle of ~ 30° between the CMA axis and the surface normal.

For the oxidation experiments, oxygen was introduced into the spectrometer chamber through a leak valve. The oxygen partial pressure was maintained at 10^{-8}–10^{-6} Torr. The partial pressure of oxygen and the purity of the gas were controlled by means of a quadrupole mass analyzer (QMA). During oxygen exposures all filaments were turned off except the QMA filament. After each oxygen exposure the filaments were turned on again while pumping off the oxygen until the initial partial pressure was reached. Then AES, XPS and/or EELS measurements were made.

3. Results

Fig. 1 shows the derivative Auger spectra of chromium in the 10–60 eV energy range for different oxygen exposures up to 40 L (1 L $\equiv 10^{-6}$ Torr s). The oxygen partial pressure was 1×10^{-8} Torr. The spectrum labelled 0 L is

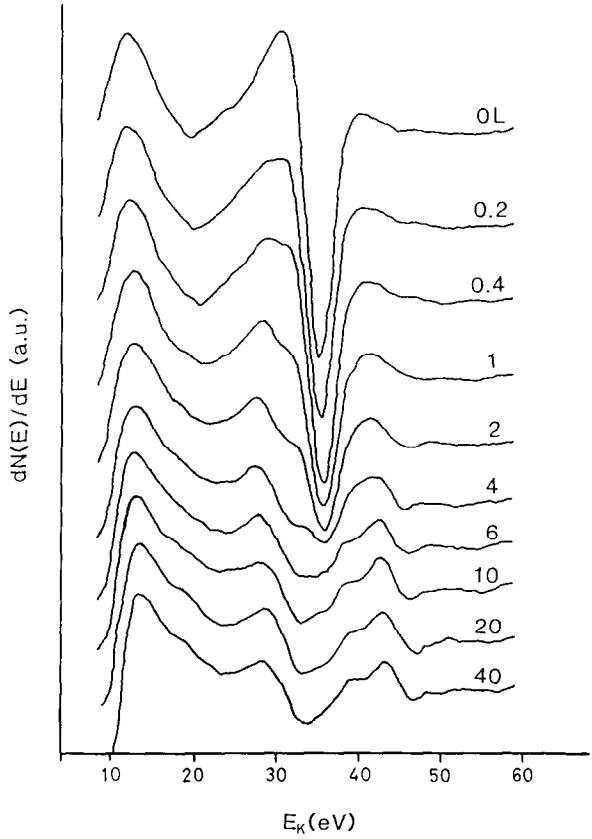

Fig. 1. Derivative CrMMM Auger spectra (arbitrary units (a.u.)) as a function of kinetic energy for different oxygen exposures.

characteristic of the clean sputtered chromium surface in agreement with the literature [1,2,11]. One notices the changes of the Auger peaks upon increasing the oxygen exposure. In order to determine the position more precisely and to follow more accurately the development of the peaks, the derivative of the spectra of fig. 1 were calculated and plotted in fig. 2. The minima in fig. 2 correspond to the maxima in $N(E)$ [2,12].

It follows from figs. 1 and 2 that the clean sputtered surface is characterized by a peak at 36.5 eV (fig. 1) in the dN/dE mode (34.5 eV in the d^2N/dE^2 mode) associated with the $CrM_{23}M_{45}M_{45}$ transition. With increasing oxygen exposure this peak is attenuated and a new peak appears on the low energy side of the $CrM_{23}M_{45}M_{45}$ peak at 33.5 eV (dN/dE mode) or 31.5 eV (d^2N/d^2E mode). This peak becomes evident at oxygen exposures as low as 0.2 L. As the oxidation proceeds (> 1 L) a peak appears at 47 eV (fig. 1). This

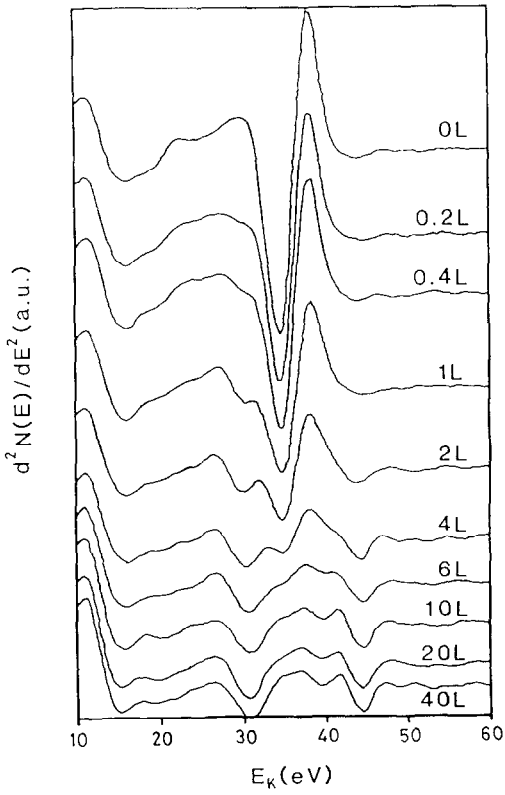

Fig. 2. Derivative of the spectra of fig. 1.

peak is coupled to another peak at ~ 40 eV which becomes clearly visible at oxygen exposures above 10 L. For exposures higher than 10 L the spectra remain unchanged indicating that a sufficiently thick layer has grown to quench completely the AES signal coming from the metallic substrate.

Fig. 3 shows the analogous XPS spectra of the Cr 2p band of the clean and of the oxygen exposed surfaces up to 10 L. One observes a chemical shift of the Cr 2p bands to higher binding energies with increasing oxygen exposures. Also, fig. 3 shows that the Cr 2p bands of the pure metal are slightly asymmetrical and that oxygen exposure increases this asymmetry.

In order to determine the oxygen exposure at which the Cr 2p band associated with Cr_2O_3 formation appears first, a deconvolution method was used consisting in subtraction of the spectrum of metallic chromium from the measured spectra of the oxidized surface. After background subtraction using the FIT version (005) of the ESAU program (Physical Electronics) based on

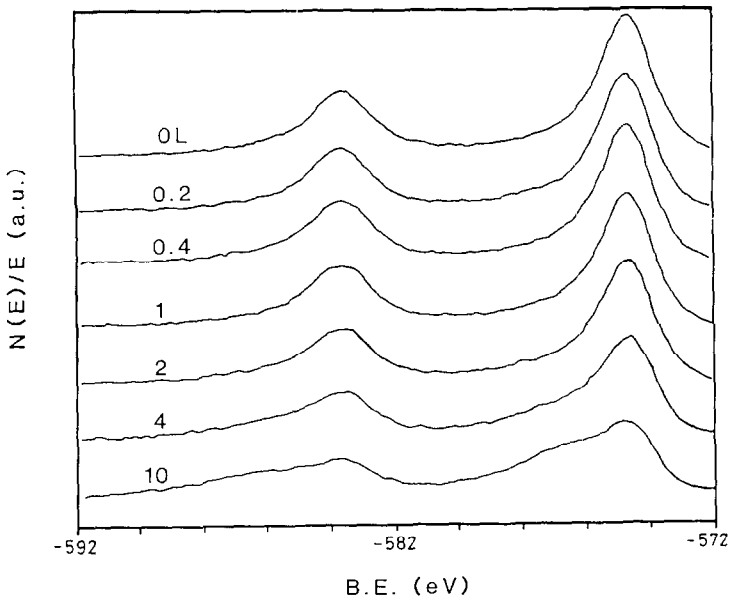

Fig. 3. XPS Cr2p spectra as a function of binding energy for different oxygen exposures.

the Shirley method, the spectra were digitized (HP-9845 computer) and the spectrum corresponding to the clean surface was normalized by a factor which minimizes (in the least squares sense) the difference. This procedure allows one to calculate the normalized attenuation of the metallic band upon oxygen exposure and it will later be used to study the kinetics of oxidation. After subtraction the data were smoothed by a subroutine of least squares fitting [13,14]. Obtained oxide spectra as well as the corresponding Cr 2p experimental raw data are shown in fig. 4 for different oxygen exposures. For oxygen exposures above 1 L the energy position of the peaks of the subtracted spectra and its area ratio $2p_{1/2}/2p_{3/2}$ are consistent with the Cr_2O_3 formation. On the other hand, the observed increase in the asymmetry of the bands for oxygen exposures $\leqslant 1$ L cannot be related to oxide formation.

Fig. 5 shows the EELS spectra, of the clean sputtered and oxygen exposed (0–10 L) Cr surfaces taken at $E_p = 500$ eV, in the $-d^2N/dE^2$ mode which has been obtained numerically from the dN/dE raw data. The maxima in $-d^2N/dE^2$ correspond to the maxima in $N(E)$ but extreme care is necessary to avoid artifacts due to differentiation [12–15]. Fig. 5 reveals changes of the shape of spectra as the oxidation proceeds. This is in agreement with the AES and XPS spectra of figs. 1–4. For the clean surface, labelled 0 L, the observed peaks are at 9, 17, 24.5, 36.7, 47.5, 57 and 77 eV respectively, in good agreement with the values reported by Sakisaka et al. [2] for the Cr(110)

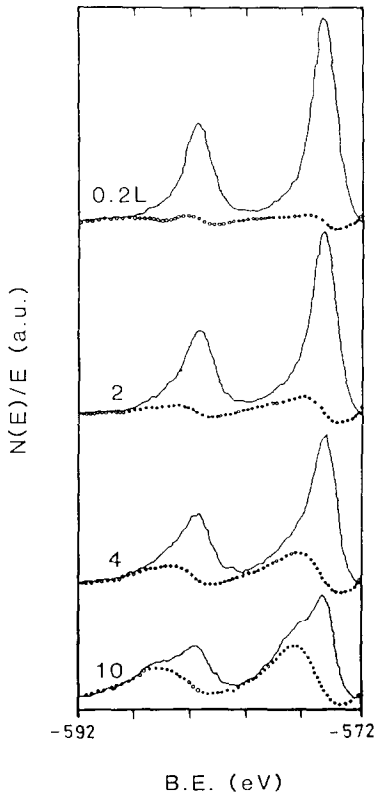

Fig. 4. XPS Cr2p spectra for different oxygen exposures. Continuous curves are the experimental data, dotted curves are the oxide spectra obtained by subtraction as explained in the text. Oxygen exposures are 0.2, 2, 4 and 10 L, respectively.

surface. In the present work the loss peaks at energies lower than 9 eV could not be resolved. The peak at 17 eV decreases as the oxidation proceeds and disappears completely for oxygen exposures above 1 L. The peak at 24.5 eV decreases similarly and becomes broader for increasing oxygen exposure. Finally, the peak at 47.5 eV splits into two new peaks, at 44.7 and 49.7 eV respectively, for oxygen exposures higher than 1 L. Above 10 L the EELS spectra remain almost invariable.

Fig. 6 shows (a) the O KLL AES peak-to-peak (ptp) intensity normalized to that at 500 L as a function of oxygen exposure (filled circles). In addition, in (b) the AES peak-to-background (ptb) intensity of the $CrM_{23}M_{45}M_{45}$ transition, I_{Cr}, normalized to the pure chromium signal. I_{Cr}^{∞}, is given (open circles). Metal and oxide chromium peaks in the 10–60 eV range overlap. Therefore, for exposures higher than 1 L, the normalized intensity ratio, I_{Cr}/I_{Cr}^{∞} has been

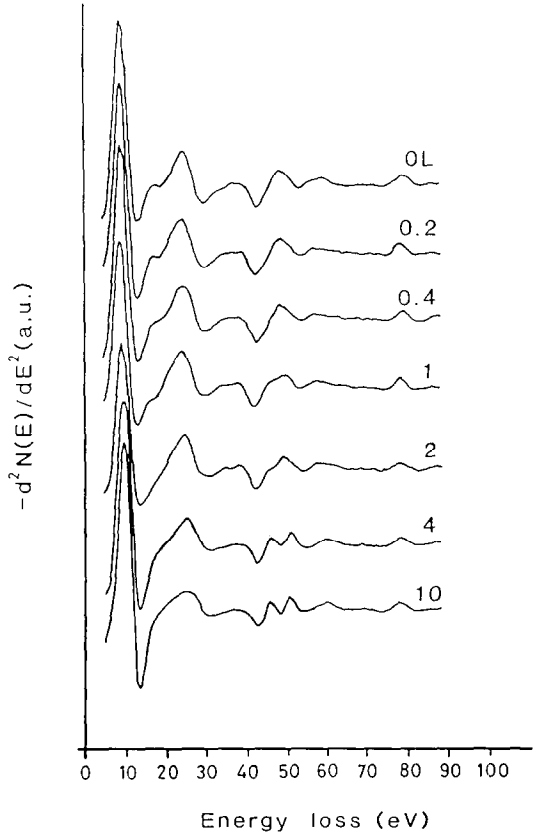

Fig. 5. Energy loss spectra, $-d^2N(E)/dE^2$, of chromium as a function of energy loss for different oxygen exposures in arbitrary units (a.u.). The energies are referenced to the elastic peak at 500 eV.

calculated by assuming that the measured spectrum, S_E, for a given oxygen exposure can be described by a linear combination of the clean surface spectrum, S_C, and the 500 L spectrum, assumed to be the oxide spectrum, S_O, since the AES data of fig. 1 showed that for exposures above 10 L the spectra remain unchanged. Therefore, we write

$$S'_E = aS_C + bS_O + c. \tag{1}$$

Applying a least squares fit between the raw data for a given oxygen exposure, S_E, and the model, S'_E,

$$\sum_{i=1}^{n} \left(S_{E_i} - S'_{E_i}\right)^2 = \min, \tag{2}$$

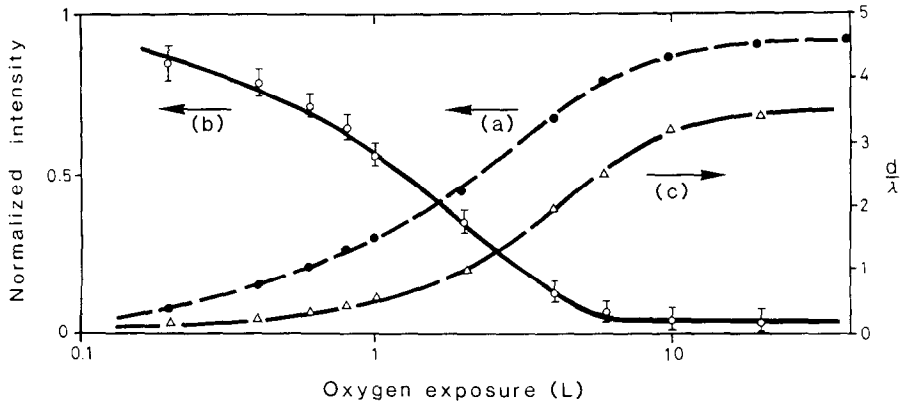

Fig. 6. AES peak-to-peak height of (a) OKLL and (b) CrMMM signal as a function of oxygen exposure. The O signals (a) are normalized to the peak-to-peak height at 500 L, the Cr signal (b) is normalized to the signal of the clean surface. (c) Relative oxide layer thickness d/λ obtained from the data of curve (b) using eq. (8). The solid line of the normalized Cr intensity (b) was calculated from eqs. (4) and (6).

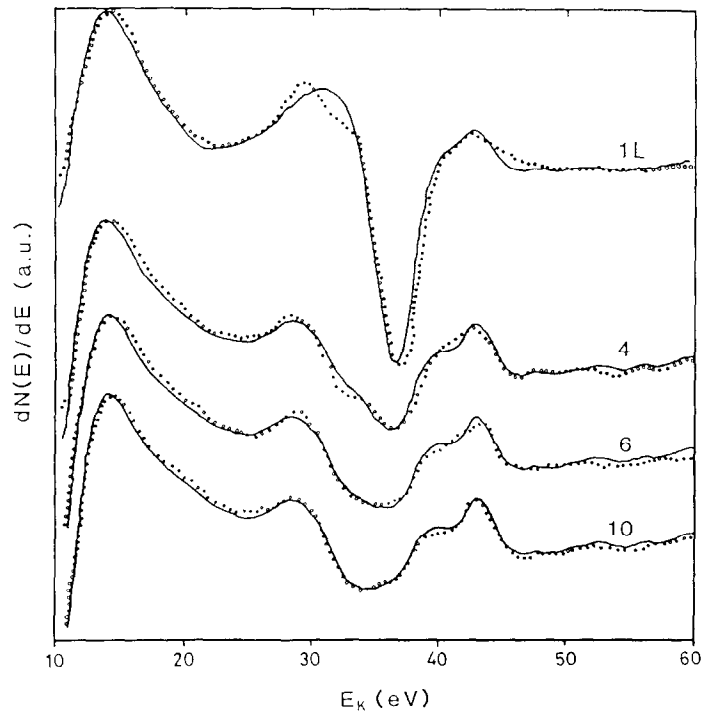

Fig. 7. Derivative CrMMM Auger spectra as a function of kinetic energy, E_K. The dotted curve represents measured values, the continuous curve the calculated spectra from eq. (1). Oxygen exposures are 1, 4, 6 and 10 L, respectively.

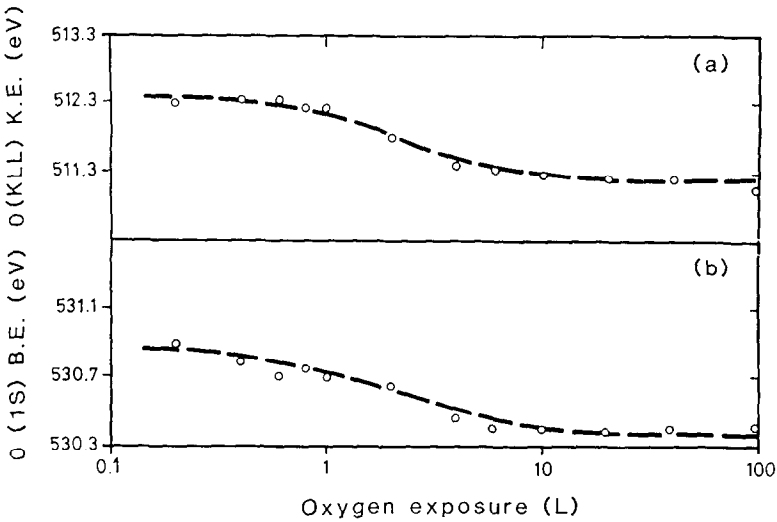

Fig. 8. Kinetic energy of OKLL AES peak (a) and binding energy of XPS O1s peak (b) as a function of oxygen exposure.

allows one to compute the parameters a, b and c, where

$$I_{Cr}/I_{Cr}^{\infty} = a \tag{3}$$

for oxygen exposures > 1 L. The results of the spectra decomposition shown in fig. 7 for increasing oxygen exposures indicate a good fit.

The evaluation of the Cr LMM transition was also followed. Upon oxygen exposure this peak shows a small shift to lower kinetic energies and broadening being due to overlap of the peaks of metallic and oxidized chromium. Since it was not possible to separate them, the Cr LMM transition was not studied further.

From the AES data of fig. 7 three different oxidation stages can be distinguished. Curves (a) and (b) show a marked change of slope at around 1 and 10 L, respectively, followed by a region of saturation. Simultaneously the O KLL kinetic energies exhibit a chemical shift as the oxidation proceeds (fig. 8a). For oxygen exposures higher than 10 L this shift amounts to 1.2 eV. For the oxygen XPS O1s peak, a shift (~ 0.5 eV) to lower binding energies is observed as the oxygen exposure increases (fig. 8b) correlating with the AES peak shift.

Three different kinetic regions are distinguished also from XPS intensity measurements. Fig. 9 shows (a) the O1s peak area as a function of the oxygen exposure normalized to the O1s peak area at 500 L and (b) the normalized attenuation of the metallic band $Cr\,2p_{3/2}$, obtained by spectra subtraction as described above, for different oxygen exposures.

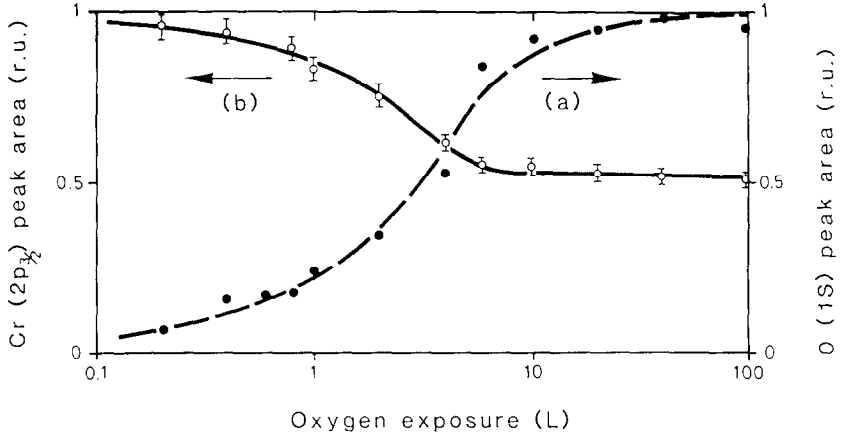

Fig. 9. Peak area (rel. units) of (a) O1s and (b) metallic Cr2p as a function of oxygen exposure. The signals are normalized to the peak area at 500 and 0 L, respectively.

It is interesting to compare the different attenuations of the $Cr\,2p_{3/2}$ (fig. 9b) and the $Cr\,M_{23}M_{45}M_{45}$ (fig. 6b) which are a consequence of the larger mean escape depth of the photoelectrons. However, the XPS data of fig. 9 indicate the same three oxidation stages, as observed by AES.

4. Discussion

The experimental data allow one to correlate changes in spectra lineshape with oxidation kinetics. The AES spectrum of the clean sputtered surface is characterized by a "metallic" peak at 36.5 eV (fig. 1). The attenuation of this peak with increasing oxygen exposure is used below to study oxidation kinetics. Exposure to oxygen causes the appearance and development of new peaks at 33.5, 40 and 47 ev, respectively. There is a controversy on the assignment of these peaks. Ekelund and Leygraf [1] found a peak at 31 eV for light oxygen exposures and a peak at 46 eV for heavier oxygen exposures. They interpreted the peak at 31 eV as due to an oxygen overlayer on the surface and the 46 eV peak as the $M_{23}VV$ transition of the oxide. Allen et al. [3] observed the 31 eV peak in conjunction with the 46 eV peak even at very low coverages (< 0.1 L). Sakisaka et al. [2] found peaks at 33 and 46 eV simultaneously but always for oxygen exposures higher than 6 L. They interpreted the peak at 33 eV as a cross transition between the chromium and the oxygen and the 46 eV as the $M_{23}VV$ transition of the oxide in agreement with Ekelund and Leygraf [1]. Because of analyzer calibration uncertainties one should not overemphasize the precision of the peak energies which is hardly

better than 1 eV. In the present work a single peak at 33.5 eV was observed for coverages smaller than ~ 1 L only. For higher oxygen exposures when XPS and EELS spectra show the presence of Cr_2O_3 (figs. 4 and 5) one observes a second peak at 47 eV. For oxygen exposures higher than ~ 6 L, the 36.5 eV metallic peak disappeares, but a new peak at 40 eV can be distinguished.

The XPS data of fig. 4 show that for exposures > 1 L the spectrum obtained by subtraction of the metallic chromium from the measured spectrum is consistent with Cr_2O_3. For exposures < 1 L neither the peak energy nor the area ratio $2p_{1/2}/2p_{3/2}$ corresponds to Cr_2O_3. The calculated spectrum for these conditions, however, differs from background noise and shows a characteristic asymmetry on the high binding energy side of the Cr 2p band. The behavior is attributed to the presence of chemisorbed oxygen on the metallic surface.

The results of fig. 5 showing the EELS spectra of clean sputtered and oxygen exposed chromium surfaces will be used as complementary information to AES and XPS measurements. Fig. 5 shows gradual changes up to ~ 1 L, before becoming more pronounced between 2 and 10 L. Beyond 10 L the EELS spectra remain unchanged. These changes correlate very well to those of AES and XPS spectra (figs. 1–4), suggesting that chemisorbed oxygen is transformed into oxide at 1–2 L in good agreement with Sakisaka et al. [2].

The data of figs. 6 and 9 show three different oxidation stages. The AES and XPS signal intensities for Cr and O plotted against oxygen exposure exhibit a marked change in slope at 1–2 L and a region of saturation above 10 L. The behavior of the O 1s signal intensity is similar to that found by Gewinner et al. [4] and Foord and Lambert [8] who studied the oxidation of chromium (111) and (110) surfaces, respectively. No comparable data showing the attenuation of the AES and XPS intensities of metallic Cr have been reported in the literature.

Oxygen uptake curves similar to those observed here have been found for other metals [16–21]. They were interpreted according to the following model [22]: (a) chemisorption of oxygen, (b) oxide island nucleation and growth until coalescence, and (c) thickening of the oxide film by transport of the reactive species through the film. A similar sequence is proposed to explain the present results for chromium oxidation. Nucleation of oxide islands on top of the chemisorbed oxygen has also been described by other authors [1,9–11] for the oxidation of the chromium (111), (110) and (100) surfaces.

Eq. (4) describes the kinetics of the first stage

$$I_{Cr} = I_{Cr}^{\infty}[(1-\theta) + \theta \exp(-1/\lambda)], \tag{4}$$

where I_{Cr}^{∞} is the signal intensity of the clean chromium substrate (peak heights in AES or peak areas in XPS), I_{Cr} the observed signal intensity, λ the electron escape depth, $\exp(-1/\lambda)$ the attenuation factor of the substrate signal due to the coverage by one monolayer of oxygen atoms, and θ the oxygen coverage

given by

$$\theta = 1 - \exp(-KL), \tag{5}$$

with L representing the oxygen exposure and K a factor relating the oxygen impingement rate to the number of adsorption sites [16,18–21].

For oxygen exposures higher than ~ 1 L the presence of chromium oxide is evidenced by all three surface analytical techniques used in this work (see figs. 1 and 3–5) in contrast to the results of Dolle et al. [7] who found that the oxidation of polycrystalline chromium starts only for oxygen exposures above 10 L. Chemical shifts of the O KLL Auger transition and of the O 1s band (fig. 8), have been observed. A similar behavior was found previously for the oxidation of Zr and Ni [16,17,23] and was attributed to a change of the oxide geometry. The chemical shifts of fig. 8 and the observed change of the slope of the oxygen uptake curves of figs. 6 and 9 are interpreted as the appearance and growth of oxide nuclei on the sample surface.

The equation which describes the lateral growth of oxide islands on a substrate covered with one monolayer (1 ML) of chemisorbed oxygen is given by [16,18–21] eq. (6)

$$I_{Cr} = I_{Cr}^{\infty}\Big\{\exp(-1/\lambda) + [\exp(-n/\lambda) - \exp(-1/\lambda)] \times \big[1 - \exp\big(-C(L - L_0)^2\big)\big]\Big\}, \tag{6}$$

where n is the average thickness (in ML) of the islands. Then the coverage of the surface by oxide islands, θ_{ox}, is given by eq. (7)

$$\theta_{ox} = 1 - \exp\big(-C(L - L_0)^2\big), \tag{7}$$

where C is a constant related to the density of nuclei [18,19] and L_0 the oxygen exposure at which the lateral growth starts. The average thickness of the island is assumed to be constant, i.e. only lateral growth is considered.

Eqs. (4) and (6) have been used to fit the experimental data for the first two stages of the oxidation. The results are shown in fig. 6 for the AES metallic peak (33.5 eV) and in fig. 9 for the $Cr\,2p_{3/2}$ metallic band by the solid lines. The fit is very good despite the simplifications of the model. The parameters leading to the best fit of the curves are shown in table 1. The values of L_0 compare well with the oxygen exposure, at which Cr_2O_3 appears according to XPS and EELS results (figs. 4 and 5). The escape depths obtained from the fit

Table 1
Best fit parameters

	λ (ML)	K (L^{-1})	n (ML)	C ($Torr^{-2}\,s^{-2}$)	L_0 (L)
AES data (fig. 6b)	1.2	1.3	3.8	2.3×10^{11}	1.1
XPS data (fig. 9b)	5.8	0.95	3.6	1.4×10^{11}	1

of figs. 6a and 9b, respectively, are of the same order of magnitude as those calculated from the empirical relations given by Seah and Dench [24] for an emission angle of 30° [29]. These values are 1.1 and 2.4 ML for the $CrM_{23}M_{45}M_{45}$ transition, and 3.4 and 5.7 ML for the $Cr2p_{3/2}$ band of the metallic and oxidized state, respectively.

The parameter C, related to the density of nuclei, is of the order of 10^{11} $Torr^{-2}$ s^{-2} (table 1). This value is comparable to the value obtained for the oxidation of Zr [16]. However, an estimation of the density of nuclei [18,19] is only possible if the temperature dependence of C is known. From the K-values of table 1 one calculates for the number of adsorption sites filled at 1 ML $N_0 \approx 1 \times 10^{19}$ atoms/cm^2 which is of the same order of magnitude as the values reported by Sakisaka et al. [2] for the atom density of Cr(110) (1.7×10^{19} atoms/cm^2) and by Gewinner et al. [4] for the atom density of Cr(111) (0.7×10^{19} atoms/cm^2). Such N_0-values can be expected for a chemisorbed monolayer.

For a homogeneous film covering the surface the signal intensity of metallic chromium is given by eq. (8) where d is the film thickness:

$$I_{Cr} = I_{Cr}^{\infty} \exp(-d/\lambda). \tag{8}$$

The film thickness at the beginning of the third oxidation stage deduced from eq. (8) should be the same as the island thickness of 3.8 ML deduced from eq. (6) for the second oxidation stage. Eq. (8) was applied to the I_{Cr} data of fig. 6

Table 2
Oxide thickness

	Crystal	Anal. tech.	Exposure (L)	Thickness (nm)
Allen et al. [3]	Cr(110)	XPS	1.16	0.37
			7.2	0.82
			67	0.82
Dolle et al. [7]	Polycrystal	XPS	Sat.(?)	1.13
Foord and Lambert [8]	Cr(100)	XPS	100	0.4
	Cr(110)	XPS	100	1.3
Gewinner et al. [4]	Cr(111)	XPS	500	0.9
	Cr(100)	XPS	Sat.(?)	0.3
Sakisaka et al. [2]	Cr(110)	AES	10	~ 0.4
This work	Polycrystal	AES	1	0.14
		AES	6	0.66
		AES	20	0.85
		XPS	1	0.19
		XPS	6	0.7
		XPS	20	0.78

and the resulting d/λ values were plotted on the same figure (curve c). Although eq. (8) is strictly applicable only for the third oxidation stage the obtained data shown that for ~ 10 L the film thickness is ~ 4 ML, consistent with the model. Table 2 compares oxide thicknesses reported in the literature with the present work assuming 1 ML = 0.21 nm. AES and XPS data agree reasonably well with the reported values.

Data for oxygen exposures above 10 L suggest a logarithmic type growth law. Although the small range of pressures studied limits the accuracy an extrapolation of the present results (fig. 9b) to exposures of 10^9 L gives a thickness of ~ 1.5 nm in agreement with Allen et al. [3]. This order of magnitude one also finds for other metals [25]. Logarithmic type growth laws are common in low temperature metal oxidation [26–28] and are usually explained in terms of the theory of Cabrera and Mott [30].

5. Conclusions

The application of AES, XPS and EELS to the study of the reaction of oxygen with a clean polycrystalline chromium surface at room temperature leads to consistent results. With increasing oxygen exposure three stages can be distinguished: chemisorption of oxygen up to 1–2 L, nucleation and lateral growth of oxide islands up to 10 L, and growth of a compact oxide film at > 10 L.

The first stage is characterized by a binding energy shift of 0.5 eV and a kinetic energy shift of 1.2 eV for the O1s and OKLL peaks, respectively, compared to the oxide.

The second stage is characterized by a much steeper slope of the oxygen uptake and chromium attenuation curves accompanied by a marked change in the AES, XPS and EELS spectra. Theoretical modelling yields an island thickness of 3.8 ML.

The third stage is characterized by a low oxidation rate which can be described by a logarithmic growth law.

Acknowledgments

The authors thank N. Xanthopoulos for technical assistance. One of us (C. Palacio) acknowledges financial support from the Spanish Education Ministry. This work is part of a research project supported by the Fonds National Suisse, Berne.

References

[1] S. Ekelund and C. Leygraf, Surface Sci. 40 (1973) 179.
[2] Y. Sakisaka, H. Kato and M. Onchi, Surface Sci. 120 (1982) 150.
[3] G.C. Allen, P.M. Tucker and R.K. Wild, J. Chem. Soc. Faraday Trans. II, 74 (1978) 1126.
[4] G. Gewinner, J.C. Peruchetti, A. Jaéglé and A. Kalt, Surface Sci. 78 (1978) 439.
[5] J.C. Peruchetti, G. Gewinner and A. Jaéglé, Surface Sci. 88 (1979) 479.
[6] G. Gewinner, J.C. Peruchetti and A. Jaéglé, Surface Sci. 120 (1982) 383.
[7] P. Dolle, M. Alnot, J.J. Ehrhardt and A. Casutto, J. Electron Spectrosc. Related Phenomena 17 (1979) 299.
[8] J.S. Foord and R.M. Lambert, Surface Sci. 161 (1985) 513.
[9] C. Jardin and P. Michel, Surface Sci. 71 (1978) 575.
[10] C. Jardin, B. Minh Duc, J.P. Gautier and P. Michel, J. Microsc. Spectrosc. Electron. 4 (1979) 55.
[11] J.P. Coad and J.C. Rivière, Phys. Letters A35 (1971) 185.
[12] C. Palacio, J.M. Sanz, Y. Casas and J.M. Matinez-Duart, to be published.
[13] F.B. Hildebrand, Introduction to Numerical Analysis (McGraw-Hill, New York, 1956) ch. 7.
[14] A. Proctor and P. Sherwood, Anal. Chem. 52 (1980) 2315.
[15] V.E. Heinrich, Appl. Surface Sci. 6 (1980) 87.
[16] J.M. Sanz, C. Palacio, Y. Casas and J.M. Martines-Duart, Surface Interface Anal., in press.
[17] R.L. Tapping, J. Nucl. Mater. 107 (1982) 151.
[18] P.H. Holloway, J. Vacuum Sci. Technol. 18 (1981) 653.
[19] P.H. Holloway and J.B. Hudson, Surface Sci. 43 (1974) 123, 141.
[20] D.F. Michell, P.B. Sewell and M. Cohen, Surface Sci. 61 (1976) 355.
[21] D.F. Mitchell, P.B. Sewell and M. Cohen, Surface Sci. 69 (1977) 310.
[22] F.P. Fehlner and N.F. Mott, Oxidation Metals 2 (1970) 59.
[23] P.R. Norton, R.L. Tapping and J.W. Goodale, Surface Sci. 65 (1977) 13.
[24] M.P. Seah and W.A. Dench, Surface Interface Anal. 1 (1979) 2.
[25] H.J. Mathieu, M. Datta and D. Landolt, J. Vacuum Sci. Technol. A3 (1985) 331.
[26] C. Palacio and J.M. Martinez-Duart, Thin Solid Films 90 (1982) 63.
[27] J.M. Sanz and S. Hofmann, J. Less-Common Metals 92 (1983) 317.
[28] K.R. Lawless, Rept. Progr. Phys. 37 (1974) 231.
[29] S. Hofmann, in: Practical surface Analysis, Eds. D. Briggs and M.P. Seah (Wiley, New York, 1983) p. 141.
[30] N. Cabrera and N.F. Mott, Rept. Progr. Phys. 12 (1949) 163.